Supporting Information

Mitigating self-discharge and improving the performance of Mg-S battery in $Mg[B(hfip)_4]_2$ electrolyte with a protective interlayer

Dasari Bosubabu[a]*, Zhenyou Li[a], Zhen Meng[a], Li-Ping Wang[a], Maximilian Fichtner[a,b]*, and Zhirong Zhao-Karger[a,b]*

[a]Helmholtz Institute Ulm (HIU) Electrochemical Energy Storage

Helmholtzstraße 11, Ulm D-89081, Germany

[b]Prof. M. Fichtner, Dr. Z. Zhao-Karger

Institute of Nanotechnology

Karlsruhe Institute of Technology (KIT)

Hermann-von-Helmholtz-Platz 1, Eggenstein-Leopoldshafen,

D-76344, Germany

Corresponding Authors

*E-mail: bosu.dasari@kit.edu

m.fichtner@kit.edu

zhirong.zhao-karger@kit.edu

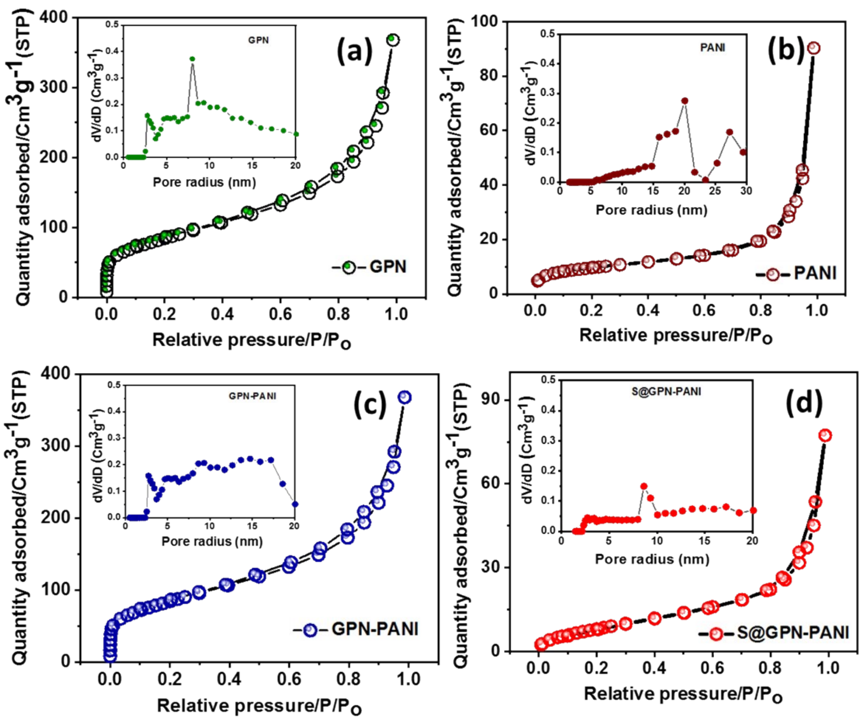

Fig. S1 Nitrogen adsorption-desorption isotherms of (a) GPN (b) PANI (c) GPN-PANI (d) S@GPN-PANI and inset of each figure shows the pore size distribution of respective material.

Table S1. Comparison of BET surface area, average pore diameter, and total pore volume of GPN, PANI, GPN-PANI, and S@GPN-PANI.

	BET surface area (m^2 g^{-1})	**Average pore diameter (nm)**	**Total pore volume (cm^3 g^{-1})**
GPN	783	7.9	0.624
PANI	32	20.4	0.102
GPN-PANI	298	12.6	0.30
S@GPN-PANI	34	9.2	0.117

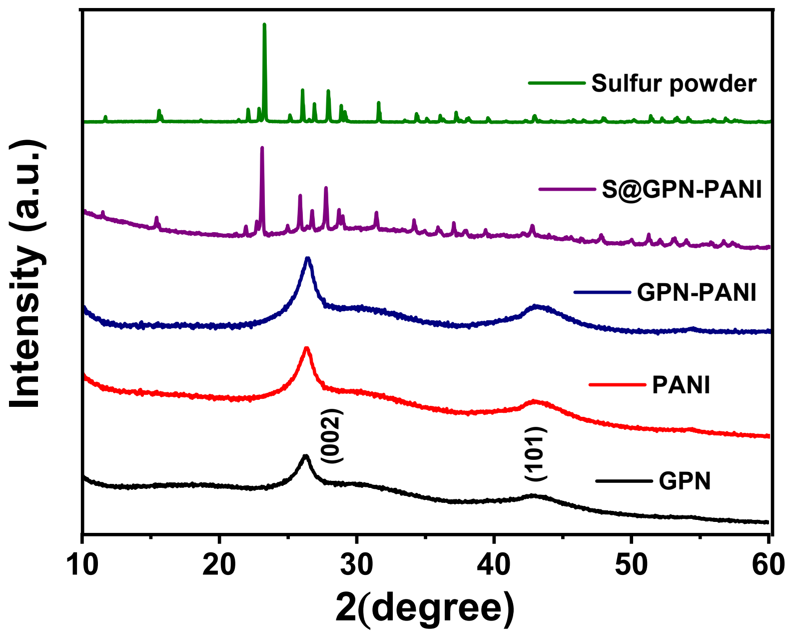

Fig. S2 The XRD pattern of GPN, PANI, GPN-PANI composite, S@GPN-PANI composite, and sulfur powder.

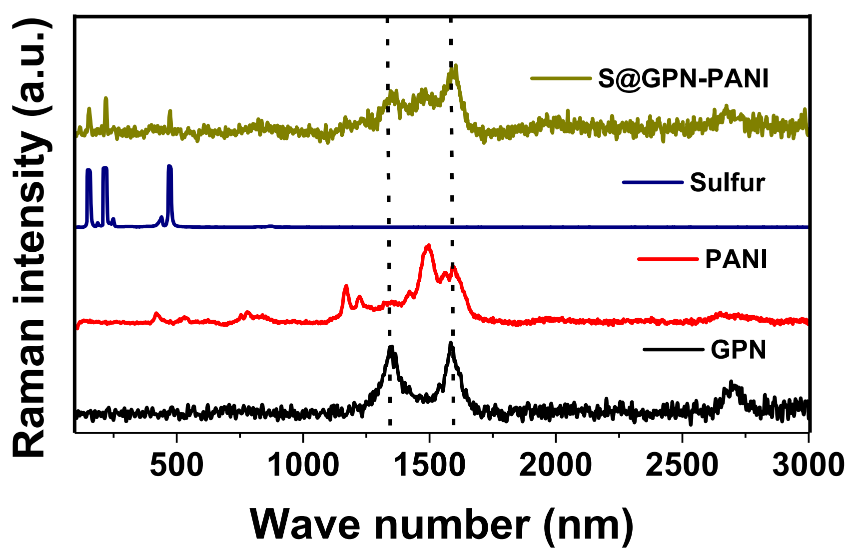

Fig. S3 The Raman spectra of GPN, PANI, sulfur powder, and S@GPN-PANI composite.

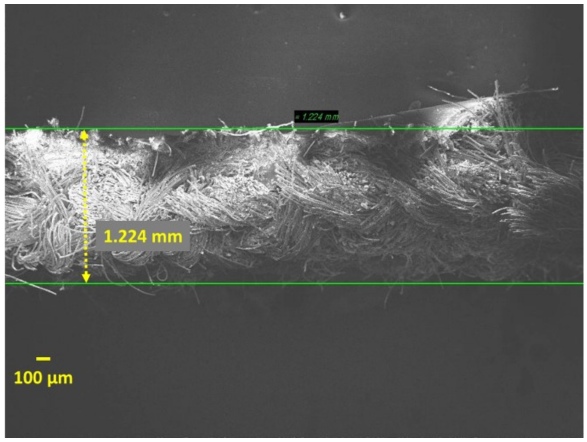

Fig. S4 The cross-section analysis of the protective interlayer

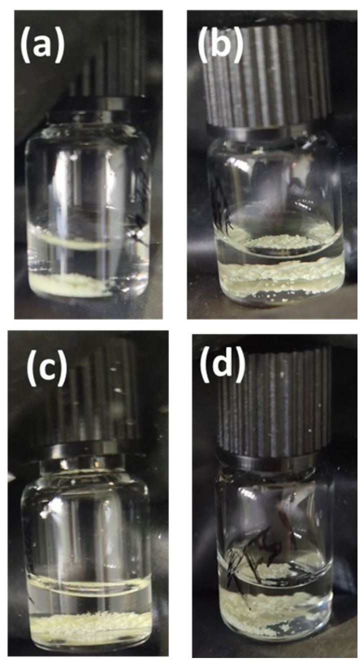

Fig. S5 Digital photo of the aging test without Mg foil both MBR and $Mg(TFSI)_2$ / $MgCl_2$ electrolyte (a, c) fresh (b, d) after 10 days of aging.

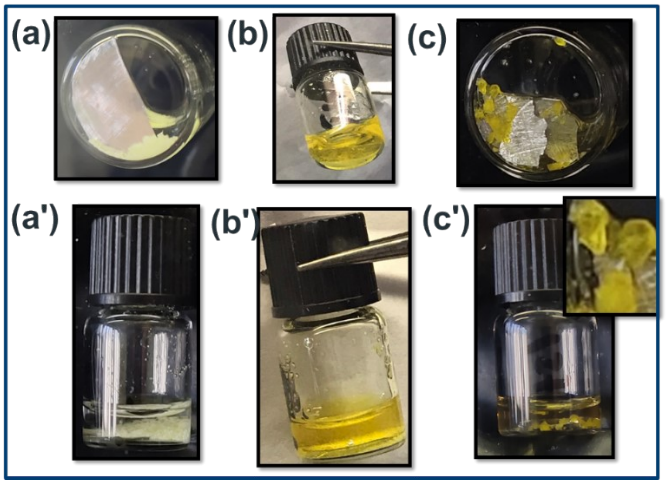

Fig. S6 Digital photo of self-discharge cell test in $Mg(TFSI)_2$ / $MgCl_2$ electrolyte (a,a') Fresh (b,b') after 24h (c,c') after 10 days.

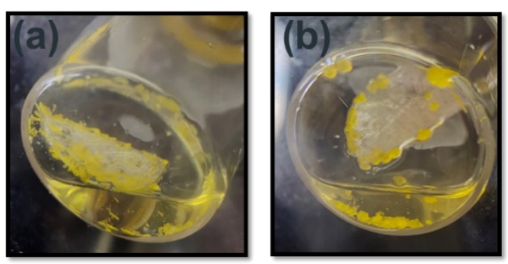

Fig. S7 Comparison of a digital photo of self-discharge cell test in (a)MBR (b) $Mg(TFSI)_2$ / $MgCl_2$ electrolyte after 10 days of the rest period.

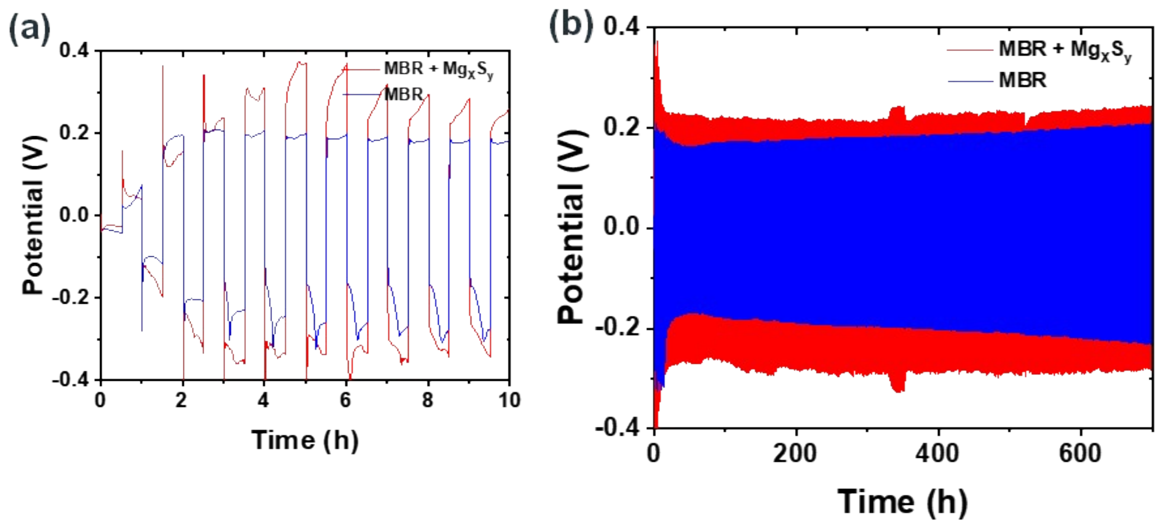

Fig. S8 (a, b) Comparison of symmetric cell Mg||Electrolyte|| Mg with and without Mg_xS_y

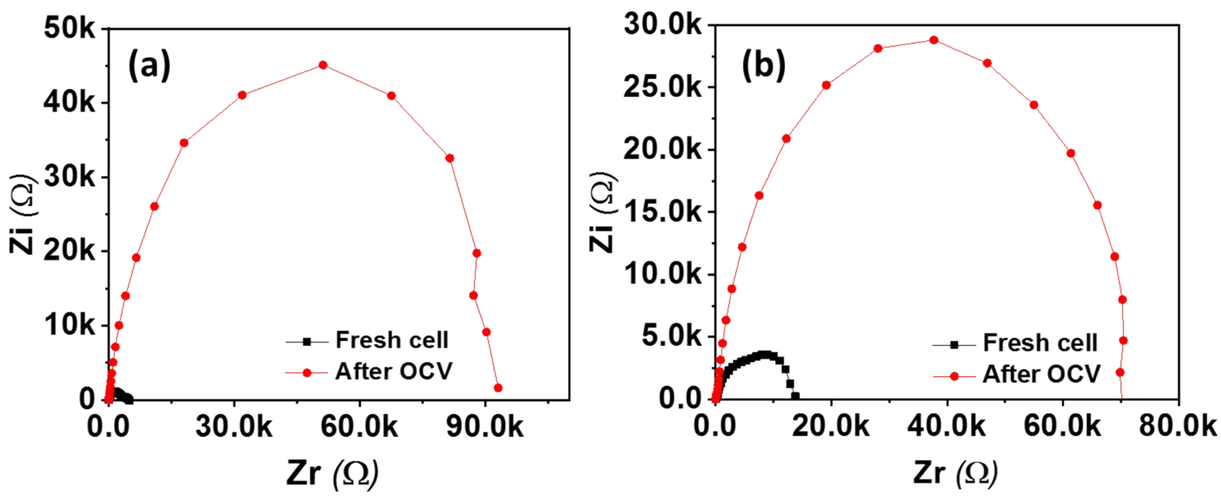

Fig. S9 Impedance of pristine cell fresh after OCV (a) CC (b) GPN-PANI@CC cell

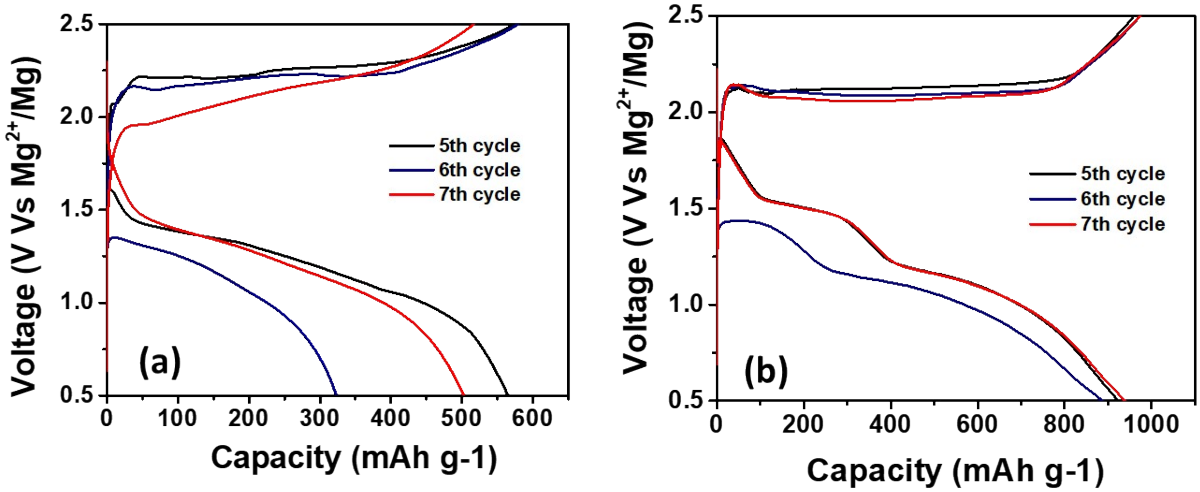

Fig. S10 Charge-discharge profile of (a) Pristine cell (b) GPN-PANI@CC interlayer cell

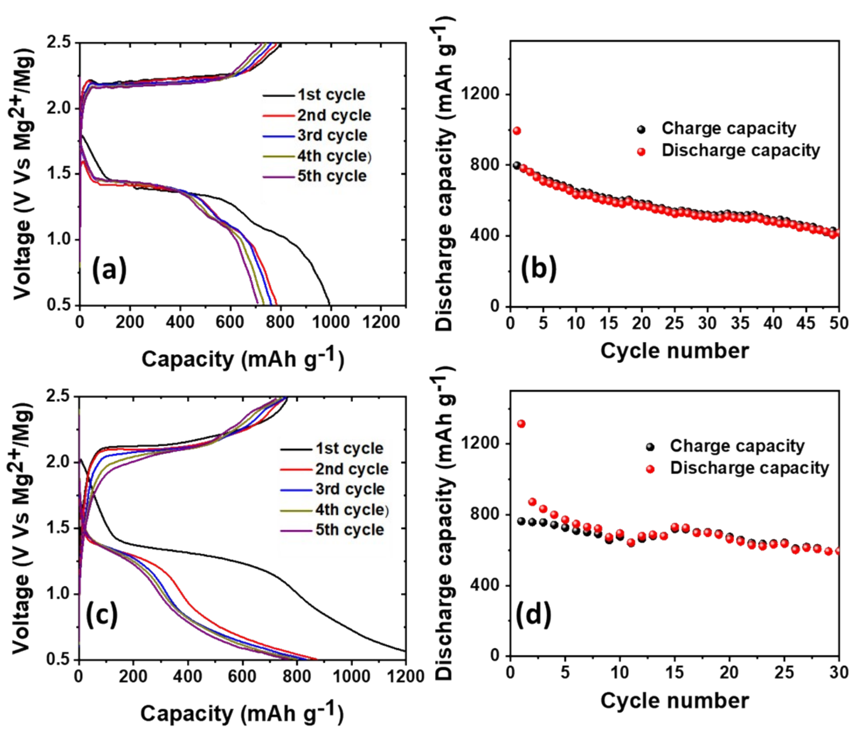

Fig. S11 Charge-Discharge profile, and electrochemical cycling performance of the GPN-PANI@CC composite (a, b) with 70% sulfur loading (c, d) with 80% sulfur loading.

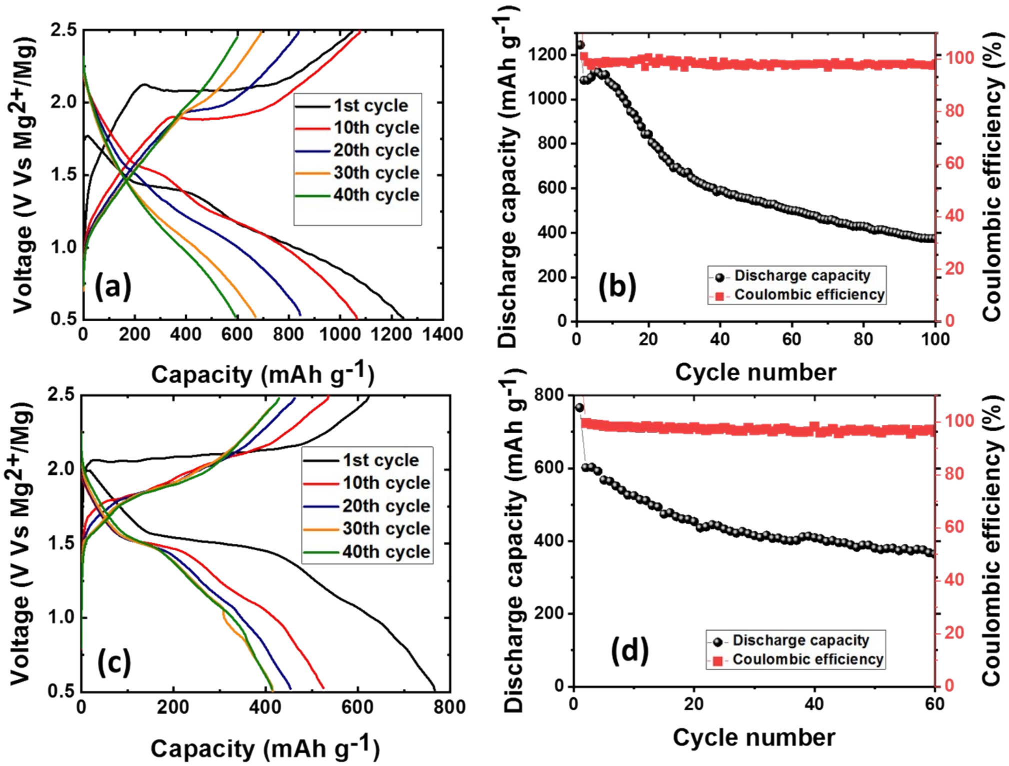

Fig. S12 (a, b) Discharge-Charge profile and capacity *Vs* cycle number profile of GPN@CC (c, d) Discharge-Charge profile and capacity *Vs* cycle number profile of PANI@CC

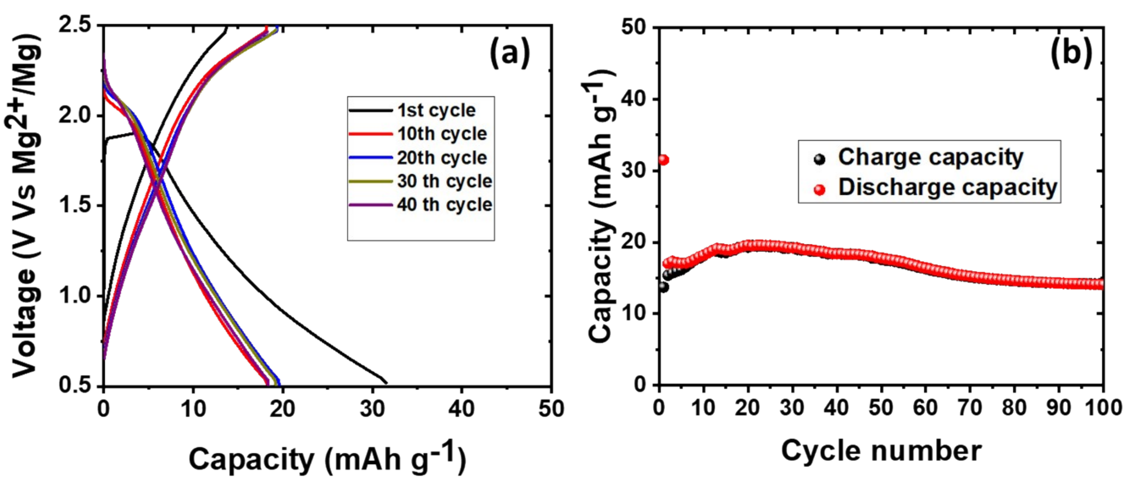

Fig. S13 Electrochemical cycling performance of the GPN-PANI composite (a) charge-discharge curve (b) capacity Vs. cycle number plot.

Fig. S14 shows the SEM and elemental mapping of cycled S@GPN-PANI@CC composite cathode coated on carbon cloth. Fig. S14 (b, c) displays Mg distribution over the electrode which confirms the sulfur becomes reduced during discharge and forms magnesium sulfide. Fig. S14 d shows the after electrochemical cycling, sulfur is re-distributed uniformly throughout the electrode

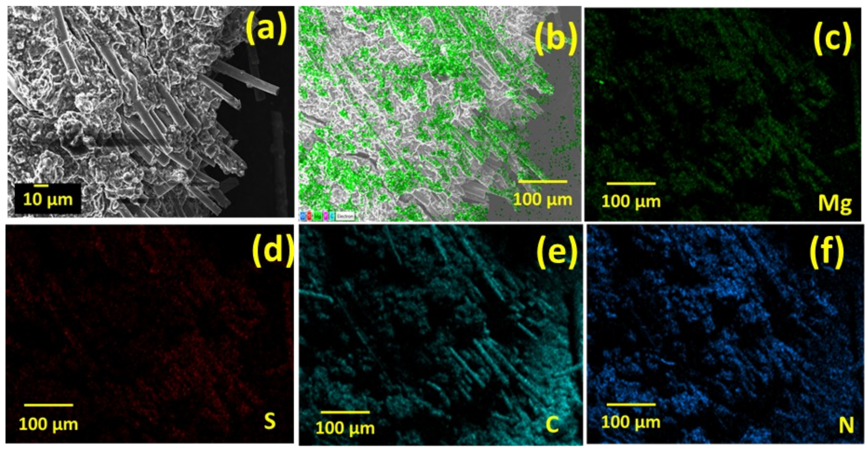

Fig. S14 (a) SEM of cycled cathode (b) Presence of Mg over the cycled electrode (c-f) Elemental mapping of magnesium, sulfur, carbon, nitrogen.

The SEM and elemental mapping of the cycled separator is also carried out where Si, O in Fig. S15 (c, d) are corresponding to the GFC separator and the S, Mg in Fig.S15 (e, f) are scattered throughout the separator are dissolved active material, these results suggest that the dissolved active material might be distributed as Magnesium sulfide on and inside the separator

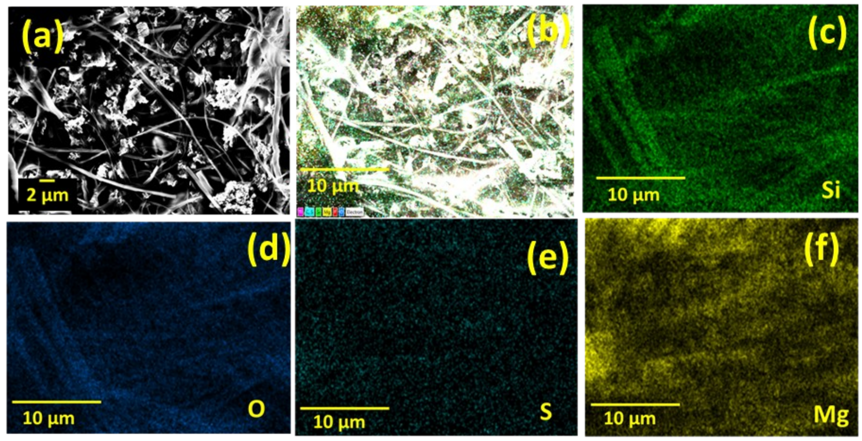

Fig. S15 (a) SEM of cycled GFC separator (b) layered overlapped elemental mapping of silicon, oxygen, sulfur, magnesium (c-f) Elemental mapping of individual silicon, oxygen, sulfur, magnesium elements.

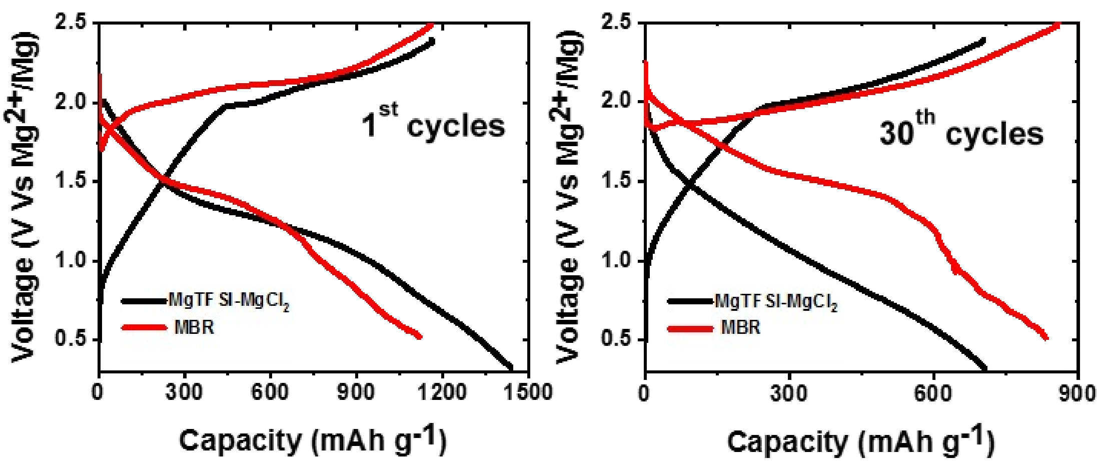

Fig. S16 GPN-PANI@CC interlayer cell comparison of charge-discharge curve in MBR, $Mg(TFSI)_2$ / $MgCl_2$ electrolyte (a) initial cycle (b) after 30 cycles.

Table S2. Comparison of GPN-PANI@CC cell electrochemical behavior with previously published Mg-S cells

S. No	**Cathode**	**Sulfur Loading [wt%]**	**Separator**	**Electrolyte**	**Coulombic efficiency [%]**	**Cell voltage**	**Capacity [mAhg^{-1} sulfur] / Initial**	**Final**	**current rate/ cycle number**	**Ref**
1	S-GO-MWCNT	0.5-3 mg cm^{-2}	PP separator	0.4 M $Mg[B(hfip)_4]_2$ /DME	>99	2.25–0.5 V	431	228	0.02C /50	[1]
2	Sulfurated poly(acrylonitrile) composite	38.3 wt%	Glass fiber	$Mg[BH_4]_2$ and $Li[BH_4]$ in diglyme	>99	0.1-1.8V	~ 1500	~ 750	0.1 C /300	[2]
3	MesoCo@C.S	0.8 mg cm^{-2}	Glass fiber	0.4 M $MgCl_2$ + $AlCl_3$ + Mg powder in DME + PYR14TFSI	~90	0.2-3.0 V	980	~ 300	0.2 C /400	[3]
4	VN/60S	60 wt%	Glass fiber	$[[Mg_2(\mu\text{-}Cl)_2(DME)_4]^{2+}$ and $[(CF_3SO_3)AlCl_3]^-$	99.1	0.4-2.0V	866	844	200 mA g^{-1} /20	[4]
5	S@ microporous carbon	55.8 wt%	PE separator	Magnesium bis (diisopropyl) amide MBA-$AlCl_3$–LiCl/ THF	94	0.5-1.7 V	700	400	0.04 C /100	[5]
6	Sulfur and KB	50 wt%	POM-electro spin coated glass fiber	0.3 M $Mg[B(hfip)_4]_2$ /DME	90	0.5-2.5 V	360	320	0.1 C /100	[6]
7	80% S@ microporous carbon on Cu	55 wt%	PE separator	0.125 M $Mg(CF_3SO_3)_2$ + 0.25 M $AlCl_3$ + 0.25 M $MgCl_2$ + 0.025 M anthracene+0.5M $LiCF_3SO_3$/THF + TG (1:1 v/v%)	90	0.5-1.7V	1194	420	0.05C /55	[7]
8	**S@ GPN-PANI@CC**	**60% wt%**	**Glass fiber**	**0.4 M $Mg[B(hfip)_4]_2$ /DME**	**>99**	**0.5-2.5 V**	**1121**	**500**	**0.1C /150**	**This work**

References

1. B. P. Vinayan, H. Euchner, Z. Zhao-Karger, M. A. Cambaz, Z. Li, T. Diemant, R. J. Behm, A. Gross and M. Fichtner, *Journal of Materials Chemistry A*, 2019, **7**, 25490-25502

2. P. Wang, J. Trück, S. Niesen, J. Kappler, K. Küster, U. Starke, F. Ziegler, A. Hintennach and M. R. Buchmeiser, *Batteries & Supercaps*, 2020, **3**, 1239-1247.
3. J. Sun, C. Deng, Y. Bi, K.-H. Wu, S. Zhu, Z. Xie, C. Li, R. Amal, J. Luo, T. Liu and D.-W. Wang, *ACS Applied Energy Materials*, 2020, **3**, 2516-2525.
4. D. Huang, S. Tan, M. Li, D. Wang, C. Han, Q. An and L. Mai, *ACS Applied Materials & Interfaces*, 2020, **12**, 17474-17480.
5. X. Zhao, Y. Yang, Y. NuLi, D. Li, Y. Wang and X. Xiang, *Chemical Communications*, 2019, **55**, 6086-6089.
6. Y. Ji, X. Liu-Théato, Y. Xiu, S. Indris, C. Njel, J. Maibach, H. Ehrenberg, M. Fichtner and Z. Zhao-Karger, *Advanced Functional Materials*, 2021, **31**.
7. Y. Yang, W. Wang, Y. Nuli, J. Yang and J. Wang, *ACS Applied Materials & Interfaces*, 2019, **11**, 9062-9072.